



Effect of boron promotion on the stability of cobalt Fischer–Tropsch catalysts

Kong Fei Tan^a, Jie Chang^b, Armando Borgna^{b,*}, Mark Saeys^{a,*}

^a Department of Chemical and Biomolecular Engineering, National University of Singapore, 4 Engineering Drive 4, Singapore 117576, Singapore

^b Institute of Chemical and Engineering Sciences, 1 Pesek Road, Singapore 627833, Singapore

ARTICLE INFO

Article history:

Received 13 October 2010

Revised 1 March 2011

Accepted 2 March 2011

Available online 8 April 2011

Keywords:

Fischer–Tropsch synthesis

Carbon deposition

Deactivation

Boron

Promotion

ABSTRACT

Density functional theory (DFT) calculations indicate that boron atoms are thermodynamically stable at step, p4g clock, and subsurface sites of a Co catalyst under Fischer–Tropsch synthesis (FTS) conditions. Moreover, the presence of boron at step and clock sites is calculated to destabilize the adsorption of carbon atoms at neighboring sites by +160 and +108 kJ/mol, respectively. The calculations hence suggest that boron promotion can selectively block the deposition, nucleation, and growth of resilient carbon species. To experimentally evaluate this concept, the deactivation of a 20 wt.% Co/ γ -Al₂O₃ catalyst promoted with 0.5 wt.% boron was studied for 200 h during FTS at 240 °C and 20 bar. Boron promotion was found to reduce the deactivation rate more than six-fold, without affecting the initial activity or selectivity. Characterization with X-ray photoelectron spectroscopy (XPS) and temperature-programmed hydrogenation (TPH) confirms that boron promotion reduces the deposition of resilient carbon species.

© 2011 Elsevier Inc. All rights reserved.

1. Introduction

Supported Co catalysts display favorable activity and high paraffin selectivity in Fischer–Tropsch synthesis (FTS), the catalytic conversion of synthesis gas to long-chain hydrocarbons [1–4]. However, they deactivate gradually during FTS [5,6], losing between 1% and 3% of their activity per day [7–9]. Because of the high cost of Co and the high loading typically required, this slow deactivation constitutes a significant technical challenge. Patents describing the removal of carbon deposits on Co FTS catalysts further illustrate the industrial relevance of deactivation [10–12], and promoters such as Ru [13] and K [14] have been reported to reduce carbon deposition during FTS.

To develop Co catalysts with improved stability, a detailed understanding of the deactivation mechanism is required. We have previously reported an experimental and computational study of the deactivation of a 20 wt.% Co/ γ -Al₂O₃ catalyst during FTS at 240 °C, 20 bar and for a H₂/CO ratio of 2 [9]. After 200 h, the Co catalyst had lost 30% of its maximum activity, and the deactivation behavior can be described by a first-order deactivation rate coefficient of $1.7 \times 10^{-3} \text{ h}^{-1}$. Characterization of the catalyst after 200 h of reaction by a combination of X-ray photoelectron spectroscopy (XPS), temperature-programmed hydrogenation (TPH), and transmission electron microscopy (TEM) indicated that both carbidic and poly-aromatic carbon species remain on the catalyst after

careful wax extraction [9]. No significant change in the catalyst dispersion could be detected by hydrogen chemisorption measurements after 200 h of FTS. In agreement with earlier studies [13,15–18], the gradual deactivation of Co catalysts was, at least partially, attributed to the deposition of resilient carbon species. An extensive evaluation of the deactivation of supported Co catalysts at 230 °C, 20 bar and for a H₂/CO ratio of 2 in a 100 barrel/day slurry bubble column demo-scale reactor was reported by Moodley et al. [15]. TPH studies of catalyst samples collected at different reaction times show a gradual accumulation of resilient carbon species. Using energy-filtered TEM, Moodley et al. furthermore showed that a significant fraction of the deposited carbon spills over to the alumina support [15]. Carbon-induced deactivation was also reported for Ru-promoted Co catalysts [13], for 20 wt.% Co/ZnO catalysts [16], and for 20 wt.% Co/SiO₂-zeolite catalysts [17]. Other deactivation mechanisms such as sintering and Co oxidation have also been observed. The relative importance of the different mechanisms depends on the catalyst parameters and reaction conditions, and is discussed in recent reviews by Saib et al. [5] and by Tsakoumis et al. [6].

The relative stability of different forms of deposited carbon on Co has been evaluated using density functional theory (DFT) [9]. DFT calculations indicate that the formation of large poly-aromatic islands and of a p4g surface carbide phase is thermodynamically highly favorable under FTS conditions. While the surface carbide phase nucleates and grows into step-edge defects, graphene strips grow out of the step-edge defects [9]. The DFT calculations further allow comparison with characterization data. The calculated C 1s core level binding energies of 284.5 and 283.4 eV for a graphene overlayer and for an extended p4g surface carbide phase,

* Corresponding authors. Fax: +65 6316 6182 (A. Borgna), +65 6779 1936 (M. Saeys).

E-mail addresses: armando_borgna@ices.a-star.edu.sg (A. Borgna), chesm@nus.edu.sg (M. Saeys).

respectively, can be compared with peaks around 284.6 and 283.0 eV in the XPS spectrum of a Co catalyst after 200 h of reaction [9].

Carbon deposition has been studied extensively for Ni catalysts, and several promoters have been proposed to enhance their stability during hydrocarbon steam reforming [19–24]. One of the earliest proposals is the addition of small amounts of sulfur compounds to the hydrocarbon feed, industrially implemented in the SPARG process [19]. The addition of small amounts of sulfur compounds is found to reduce the deactivation rate more than it affects the activity during steam reforming [19]. Detailed studies indicate that sulfur atoms bind strongly to step edges and hence reduce the number of nucleation sites for the growth of graphitic carbon [25]. More recently, Au [20], Sn [22], and B [23,24] have been proposed as promoters to enhance the stability of Ni catalysts during steam reforming. The relative stability of boron and carbon at different adsorption sites was calculated to be similar, and boron atoms were proposed to block the nucleation of resilient carbon deposits [23]. In addition, DFT calculations suggest that subsurface boron atoms induce a minor reconstruction of the Ni(1 1 1) surface, which reduces the methane activation barrier [26]. Experimentally, the addition of 1.0 wt.% boron to a 15 wt.% Ni/ γ -Al₂O₃ catalyst was found to reduce the first-order deactivation rate coefficient by a factor of 3 and the amount of deposited carbon by 80%, without affecting the initial catalyst activity during methane steam reforming [27].

In this work, we evaluate whether the promoting effect of boron can be extended to supported Co FTS catalysts. First, we report DFT calculations to determine the stability of boron at different Co adsorption sites under FTS conditions and to test the effect of boron on the stability of neighboring carbon atoms. Next, boron-promoted 20 wt.% Co/ γ -Al₂O₃ catalysts are prepared and characterized. Finally, the activity and stability of the boron-promoted Co catalysts are tested in a micro fixed-bed reactor at typical FTS conditions. The conclusions of this work are summarized in Section 4.

2. Computational and experimental methods

2.1. Computational details

Boron and carbon chemisorption energies were calculated using periodic spin polarized DFT and the Perdew–Burke–Ernzerhof functional (DFT–PBE) [29] as implemented in the Vienna Ab initio Simulation Package (VASP) [30,31]. Plane waves with a kinetic energy up to 450 eV were used in the calculations, and the electron–ion interactions were described by the projector-augmented wave (PAW) method [32]. Binding energies were calculated using eq. (1).

$$\text{Binding energy} = \frac{1}{N_x} [E_{(X/Co)} - E_{(Co, \text{clean})} - N_x E_{(X)}] \quad (1)$$

where $E_{(X/Co)}$, $E_{(Co, \text{clean})}$, and $E_{(X)}$ represents the total DFT–PBE energy for the combined adsorbate/Co system ($X = B$ or C), for the clean surface, and for the free atom, respectively, and N_x is the number of boron or carbon atoms per unit cell.

Co terraces were modeled with a 3-layer fcc Co(1 1 1), $p(2 \times 2)$ slab where the bottom layer was constrained at the optimized bulk Co lattice constant of 3.52 Å [33]. Although the hcp structure is preferred for bulk Co, the fcc structure is more stable for crystallites below 100 nm [34]. Step sites were created by removing 2 or 4 rows of Co atoms from the top layer of a $p(2 \times 8)$ or $p(4 \times 8)$ slabs [9]. A $(5 \times 5 \times 1)$ Monkhorst–Pack grid was used to sample the Brillouin zone for the $p(2 \times 2)$ unit cells, while a $(2 \times 2 \times 1)$ grid was used for the larger $p(2 \times 8)$ and $p(4 \times 8)$ unit cells. Repeated slabs were separated by 10 Å to minimize interactions

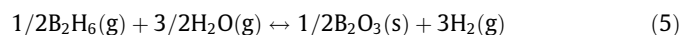
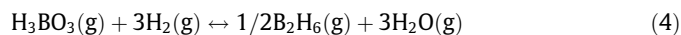
between slabs. Binding energies were found to be converged within 5 kJ/mol with respect to the vacuum spacing and the k -point sampling. Increasing the slab thickness from 3 to 5 layers reduced the carbon binding energy at the hollow site by 7 kJ/mol and the boron binding energy by 5 kJ/mol.

To evaluate the stability of adsorbed boron and carbon under FTS conditions, reaction free energies, ΔG_r (500 K, 20 bar), were calculated with reference to a gas phase reservoir of CO, B₂H₆, H₂, and H₂O at partial pressures of 4.4, 1.0, 8.9, and 6.7 bar respectively, using reactions (2) and (3). The CO, H₂, and H₂O partial pressures correspond to FTS conditions for an average CO conversion of 60%.



Gibbs free energies for the gas phase species were obtained by combining DFT–PBE electronic and zero point energies with experimental enthalpy and entropy corrections [35]. For chemisorbed carbon and boron, only the electronic energy was included in the Gibbs free energy calculation [9,28].

Diborane (B₂H₆) was used as the reference gas phase boron species since FTS is performed under reducing conditions [26,28]. Under FTS conditions, B₂H₆ is significantly more stable than boric acid, H₃BO₃, with an experimental gas phase free energy of reaction, ΔG_r , of –81 kJ/mol for reaction (4) [35]. As described below, H₃BO₃ is used to introduce the boron promoter. Bulk boron oxide (B₂O₃) on the other hand is slightly more stable than B₂H₆ under FTS conditions, with a ΔG_r of –23 kJ/mol for reaction (5) [35].



To allow comparison with the XPS data, boron 1s core level binding energies were calculated for various surface boron species using the final state approximation procedure [36]. The accuracy of the calculated core level binding energies has been estimated to be 20–50 meV [36].

2.2. Catalyst synthesis and testing

Supported cobalt catalysts were prepared by slurry impregnation of a γ -Al₂O₃ support (surface area of 380 m²/g) with an aqueous Co nitrate solution (Co(NO₃)₂·6H₂O, Sigma–Aldrich, 98%) to produce Co loadings of about 20 wt.%. The slurry was dried for 3 h at 80 °C and 80 mbar in a rotor evaporator (Buchi R-205) with a temperature-controlled bath (Buchi B-490), and overnight in an oven at the same temperature. The catalyst sample was subsequently heated to 400 °C at 1 °C/min and calcined in flowing air at 400 °C for 2 h using an electric furnace (Carbolite RWF 1200) [9]. Small amounts (0.05 wt.%) of platinum (Pt(NH₃)₄(NO₃)₂, Sigma–Aldrich, 99%) were introduced during the slurry impregnation step to improve the reducibility of the Co catalyst [7,9,37]. The boron promoter was introduced by a second slurry impregnation step using aqueous boric acid (H₃BO₃, Sigma–Aldrich, 99%) to produce boron loadings of 0.5 and 2.0 wt.%. As a control sample, the γ -Al₂O₃ support without Co was loaded with 2.0 wt.% boron. The amount of boron present after calcination and after FTS was confirmed using inductively coupled plasma–optical emission spectrometry (ICP–OES). In all cases, the measured Co:B bulk atomic ratios differ by less than 5% from the theoretical values of 1:0.13 and 1:0.55.

The catalytic performance of the catalysts was tested in a fixed bed micro-reactor with an internal diameter of 2.0 cm and equipped with a three-zone heater with three independent thermocouples. An additional thermocouple was placed inside a thermowell to measure the temperature inside the catalyst bed.

To minimize possible temperature gradients, 1.0 g of catalyst with a particle size between 212 and 300 μm was diluted with approximately 18 g of SiC with the same particle size [9]. With this setup, temperature gradients over the 5.0-cm catalyst bed were measured to be less than 1 $^{\circ}\text{C}$ during FTS at 240 $^{\circ}\text{C}$, and no hot spots were detected. Furthermore, the temperature in the bed remained constant during the entire experiment. The absence of radial thermal gradients for the 2.0-cm-diameter reactor was confirmed by Mears' criterion [38], using a conservative estimate for the effective thermal conductivity for a stagnant fluid in a packed bed [39]. The absence of mass transfer limitations was evaluated using the Weisz–Prater criteria. The calculated Weisz modulus Φ of approximately 0.14 is lower than the critical value of 1.0. The absence of internal mass transfer limitations was further tested experimentally using larger catalyst particles (300–400 μm) [9]. No significant difference in the CO conversion and selectivity could be detected between the smaller and the larger catalyst particles. Catalysts were reduced in the reactor for 12 h under 50 Nml/min H_2 at 500 $^{\circ}\text{C}$ and at atmospheric pressure. After reduction, the reactor was cooled to 120 $^{\circ}\text{C}$ under flowing H_2 . Next, syngas with a H_2/CO ratio of 2 was introduced at a $W_{\text{cat}}/F_{\text{total}}$ of 7.5 $\text{g}_{\text{cat}} \text{h}/\text{mol}$ (H_2 , Soxal, 99.9%, and a CO/Ar mixture with 95% CO and 5% Ar as internal standard, Soxal), and the reactor was brought to 20 bar and 240 $^{\circ}\text{C}$ with a slow heating rate of 0.5 $^{\circ}\text{C}/\text{min}$. The temperature of 240 $^{\circ}\text{C}$ was selected to slightly enhance the deactivation rate in order to facilitate the evaluation of catalyst promoters. Similar reaction conditions can be found in the literature [9,40–42].

The light products were analyzed online with an Agilent GC 6890, while condensed waxes were analyzed offline with a high temperature Shimadzu GC 2010 to determine yields for the C_{20} – C_{80} hydrocarbons. The mass and carbon balance could be closed to between 95% and 99% in all experiments. The catalysts were tested for 200 h, after which the reactor was cooled to 120 $^{\circ}\text{C}$ under flowing synthesis gas. The catalysts were removed from the reactor inside a glove box and separated from the SiC particles with a magnet. The absence of a Si 2s peak in the survey XPS spectrum indicated that the separation was successful. Condensed waxes were extracted with hexane [9,43] prior to the characterization studies. While solvent extraction under mild conditions may not remove all the waxes, they could be reduced to very low residual levels as indicated by the TPH and XPS data.

2.3. Catalyst characterization

To evaluate the effect of boron on the reducibility of the cobalt catalyst, temperature-programmed reduction (TPR) profiles were collected for the different catalysts in a Quantachrome Autosorb 1C with a thermal conductivity detector. Approximately 0.2 g of calcined catalyst was loaded in a U-shaped cell, dried at 120 $^{\circ}\text{C}$ for 1 h, heated in flowing air to 400 $^{\circ}\text{C}$ at 5 $^{\circ}\text{C}/\text{min}$, and kept at 400 $^{\circ}\text{C}$ for 1 h to ensure complete decomposition of the nitrate precursors. After cooling to 25 $^{\circ}\text{C}$, the TPR profile was recorded in 50 Nml/min 5% H_2/Ar up to 850 $^{\circ}\text{C}$ at 10 $^{\circ}\text{C}/\text{min}$. The catalyst dispersion and H_2 uptake were determined by H_2 chemisorption in a Quantachrome Autosorb 1C. Approximately 0.2 g of catalyst was loaded in a quartz cell, reduced in 50 Nml/min H_2 at 500 $^{\circ}\text{C}$ for 2 h, evacuated for 1 h, and cooled to 25 $^{\circ}\text{C}$ under vacuum. H_2 adsorption isotherms were measured at 25 $^{\circ}\text{C}$ between 80 and 800 mbar. The dispersion was calculated assuming a H:Co stoichiometry of 1. The dispersion for boron-promoted catalysts was determined following the same procedure, assuming that boron does not contribute to the H_2 uptake. The average particle diameter $d(\text{Co})$ was obtained from the dispersion (D) using Eq. (6) [44].

$$d(\text{Co}) [\text{nm}] = \frac{96}{D [\%]} \quad (6)$$

The particle size was determined independently from the width of the Co_3O_4 X-ray diffraction (XRD) peak at 36.8 $^{\circ}$ using Scherrer's formula [45]. XRD patterns were measured in a Bruker D8 advance diffractometer. The average Co_3O_4 particle size obtained from XRD was converted to the corresponding reduced Co particle size using the ratio of the molar volumes of metallic Co and Co_3O_4 [46]:

$$d(\text{Co}) = 0.75d(\text{Co}_3\text{O}_4) \quad (7)$$

The effect of boron promotion on the adsorption of the second reactant, CO, was evaluated with *in situ* diffuse reflectance infrared Fourier transform spectroscopy (DRIFTS). CO adsorption spectra were collected with a Perkin-Elmer FTIR 2000 spectrometer, equipped with a temperature controlled Harrick "Praying Mantis" DRIFTS cell. Approximately 50 mg of catalyst, diluted with dry KBr (1:5 w/w) to improve the signal to noise ratio, was placed in the DRIFTS cell. The catalyst samples were dried in He at 150 $^{\circ}\text{C}$ for 1 h, and reduced in 50 Nml/min H_2 for 2 h at 400 $^{\circ}\text{C}$, the maximum temperature for the cell. After exposure to a 50 Nml/min 2% CO/Ar mixture at room temperature and atmospheric pressure, infrared spectra with a resolution of 4 cm^{-1} were collected between 500 and 4000 cm^{-1} and averaged over 50 scans.

To evaluate the nature of the boron promoter on the Co catalyst after reduction, XPS spectra were collected with a Thermo ESCA-LAB 250 spectrometer. The calcined catalyst was reduced *ex situ* using a procedure developed for Ni catalysts [27]. First, the catalyst was heated to 120 $^{\circ}\text{C}$ at 5 $^{\circ}\text{C}/\text{min}$ and held at this temperature for 1 h under flowing Ar to remove adsorbed moisture. The catalysts were then heated to 500 $^{\circ}\text{C}$ at 5 $^{\circ}\text{C}/\text{min}$ under 50 Nml/min H_2 and reduced at this temperature for 2 h. After reduction, the catalysts were purged with 50 Nml/min Ar at 500 $^{\circ}\text{C}$ and cooled to room temperature. Thereafter, the catalysts were kept under an Ar atmosphere and transferred to the XPS sample holder inside a glove box with less than 0.1 ppm of water or oxygen. Finally, the samples were transferred to the XPS chamber without exposure to air [9,27]. XPS measurements were recorded with a 20-eV pass energy, a 0.1 eV kinetic energy step, and a 0.1-s dwelling time. Energy corrections were performed using the Al 2p peak of Al_2O_3 at 74.3 eV. To determine the nature of resilient carbon species remaining after FTS, catalyst samples were transferred to the XPS chamber after wax extraction, following the above procedure.

TPH was used to evaluate the effect of boron promotion on the amount and the reactivity of the deposited carbon. After wax extraction, approximately 20 mg of catalyst was loaded in a quartz tube, kept under 50 Nml/min Ar at 200 $^{\circ}\text{C}$ for 1 h to remove weakly adsorbed hydrocarbons, and cooled to room temperature. Next, 50 Nml/min H_2 was introduced and the temperature was increased to 600 $^{\circ}\text{C}$ at 5 $^{\circ}\text{C}/\text{min}$. The CH_4 signal was monitored with a Hiden HPR 20 mass spectrometer.

3. Results and discussion

First, the stability of boron on Co terraces and at step sites is evaluated using DFT–PBE. Next, the effect of boron at step and at p4g clock sites on the stability of carbon at neighboring sites is calculated. The calculations indicate that similar to carbon, boron induces a p4g clock reconstruction initiating from the step edges. Furthermore, boron at p4g clock sites reduces the stability of nearby carbon atoms and hence destabilizes the formation of resilient carbon deposits at the step edges. Based on this mechanistic insight, boron is proposed as a potential promoter to enhance the stability of Co catalysts. In order to evaluate the theoretical predictions, a series of 20 wt.% Co/ γ - Al_2O_3 catalysts were promoted with various amounts of boron, characterized and tested in a fixed bed micro-reactor for 200 h during FTS. After FTS, the catalysts were

characterized by TPH and C 1s XPS to evaluate the amount and nature of the resilient carbon deposits.

3.1. Computational study of the stability of boron on a Co surface

Boron binding energies and thermodynamic stabilities at terrace and step sites are summarized in Table 1. Similar to carbon, on-surface boron adsorbs preferentially at the hcp hollow site on Co(1 1 1). However, surface boron atoms are calculated to be unstable under FTS conditions and can gain stability by hydrogenation to B₂H₆. At a low coverage, subsurface boron is even less stable than on-surface boron. However, while the surface binding energy gradually decreases from –535 to –519 kJ/mol with increasing coverage, the binding energy at the subsurface octahedral sites gradually increases from –519 to –616 kJ/mol. Already at 0.5 ML coverage, the subsurface sites are preferred over the surface sites. Additional calculations with a larger $p(2 \times 8)$ unit cell further confirm the gradual increase in subsurface boron binding energies when two subsurface boron atoms are gradually brought closer to each other. This suggests that subsurface boron atoms prefer to form subsurface clusters rather than distribute evenly, as was also calculated for a Ni(1 1 1) surface [26]. At high concentrations, subsurface boron atoms in neighboring octahedral sites can interact. This interaction greatly increases the stability of subsurface boron to –53 kJ/mol and subsurface boron becomes 30 kJ/mol more stable than bulk boron oxide (B₂O₃) [28]. A similar effect was found for subsurface boron on Ni(1 1 1), where a high concentration of subsurface boron is 76 kJ/mol more stable than on-surface boron [23,26]. The boron–boron interaction leads to a minor surface reconstruction for both Co(1 1 1) and Ni(1 1 1), whereby boron atoms in neighboring octahedral sites form rows of boron pairs and raise the Co and Ni surface atoms between them [26,28]. The resulting structure is illustrated in Table 2. The critical concentration that leads to this minor surface reconstruction on both Co(1 1 1) and Ni(1 1 1) surfaces appears to be close to 1.0 ML. Indeed, the structures for 0.75 ML and 0.5 ML in Table 1 do not show a surface reconstruction.

Next, the stability of boron was evaluated for a stepped Co surface. Boron binds strongly at B5 step sites for a low step coverage, and the driving force to move from the surface sites to the step sites is 116 kJ/mol. This value is larger than the driving force calculated for carbon, 89 kJ/mol [9]. At a low coverage, the stability of boron at the hcp hollow site near the step edge, +20 kJ/mol, is comparable to the value calculated for the Co(1 1 1) terraces, +28 kJ/

mol. At a higher coverage, boron atoms placed initially at the hcp hollow site near the step edge relax to induce a p4g clock reconstruction. In a p4g clock reconstruction, the surface atoms undergo small displacements to create a regular mixture of 3- and 4-fold hollow sites [47]. The increased boron binding energy at the 4-fold hollow site more than compensates the energy cost for this reconstruction. The boron atoms at the fourfold hollow sites are nearly co-planar with the surface Co atoms and also interact with the Co atom below the hcp hollow site. A similar reconstruction is also favorable for carbon on stepped Co [9] and Ni [26] surfaces, as well as for boron on a stepped Ni surface [26]. Again, calculations show that the chemisorption properties of boron and carbon are similar.

Since boron atoms bind strongly near step sites, the adsorption of additional boron atoms on a stepped Co surface is explored next. Various combinations are shown in Table 2. For two boron atoms in a $p(2 \times 8)$ unit cell, the configuration with both boron atoms at p4g clock sites is more stable than the configuration with one atom at the step site and one at a p4g site. This is surprising since step sites are slightly preferred over p4g clock sites for individual boron atoms (Table 1). However, the binding energy at a p4g site consists of an energy cost to reconstruct the step edge, +77 kJ/mol for the near-edge p4g site, and a strong binding energy of –665 kJ/mol at the reconstructed 4-fold hollow site. The energy cost to form the first p4g clock site is rather high, leading to a relatively low binding energy of –588 kJ/mol for the near-edge p4g site (Table 1). The reconstruction energy cost for the second and the third p4g clock site are significantly lower at 30 and 34 kJ/mol, respectively, and the overall binding energies hence increase to –634 kJ/mol for the second row of boron and to about –632 kJ/mol for the third, fourth, and fifth row. The binding energy at the reconstructed step sites also increases from –590 to –618 kJ/mol for a single row of boron at the p4g clock sites, and to about –616 kJ/mol for a fully developed p4g clock reconstruction. However, the increase in the binding energy for the step sites is smaller than for the p4g sites. An extended p4g clock boride is hence 60 kJ/mol of boron more stable than B₂H₆ and 37 kJ/mol of boron more stable than bulk B₂O₃ under FTS conditions. The stability of the p4g surface boride, –59 kJ/mol is comparable with the stability for a monolayer of subsurface boron after a surface reconstruction, –53 kJ/mol (Table 1). To evaluate the stability of subsurface boron near the step edges, two different model structures consisting of five rows of subsurface boron were studied (Table 2). In the first structure, all the boron atoms occupy subsurface octahedral sites. The calculated stability, –54 kJ/mol, is similar to the value calculated for the terraces (Table 1). The structure in Table 2 also illustrates the Co(1 1 1) surface reconstruction, whereby one row of Co atoms is raised by 0.64 Å. The second structure with four rows of octahedral boron and one row of boron at the step sites is significantly less stable. Indeed, the boron binding energy at the step edges is only –567 kJ/mol, in agreement with the low boron binding energy for a step coverage of 100%.

The formation of a surface cobalt boride is hence thermodynamically favorable after impregnation and reduction of the boron-promoted Co catalysts. The experimental B 1s XPS spectra for the promoted Co catalysts after reduction at 500 °C indeed show a peak around 188.1 eV, consistent with the B 1s core level binding energy calculated for the p4g clock structure, 187.8 eV. A B 1s core level binding energy of 187.0 eV was calculated for a monolayer of subsurface boron for reconstructed surface, while a binding energy of 186.5 eV was calculated for boron at the B5 step sites. Both values are slightly lower than the experimentally observed peak value. To illustrate the accuracy of the core level binding energy calculations, we also computed the core level binding energy for the bulk cobalt boride structure, Co₂B [48]. The calculated binding energy of 188.2 eV is in good agreement with the experimental value of 188.1 eV [49].

Table 1

Boron binding energies and Gibbs free reaction energies under FTS conditions, ΔG_r (500 K, 20 bar), for Co terraces and for a stepped Co surface.

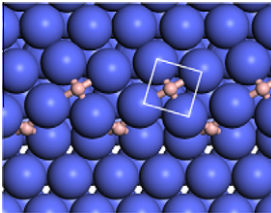
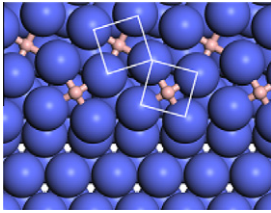
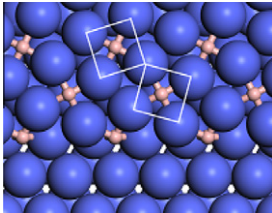
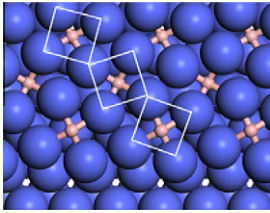
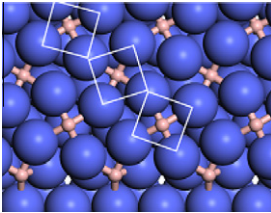
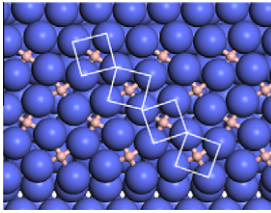
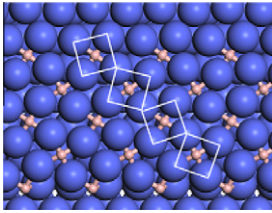
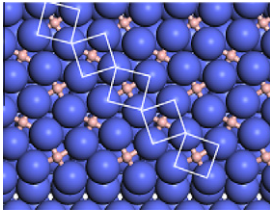
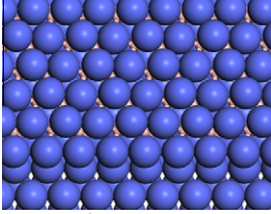
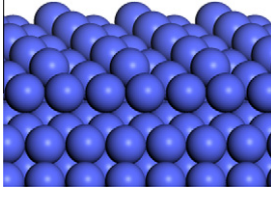
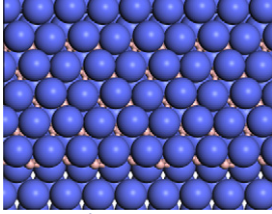
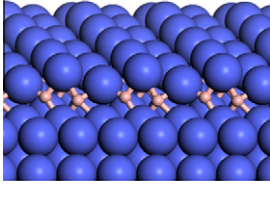
Adsorption site	Binding energy/ ΔG_r^a (kJ/mol)			
<i>Terrace sites</i>				
Coverage	0.25 ML	0.50 ML	0.75 ML	1.0 ML
On-surface (hcp hollow)	–535/+28	–528/+33	–522/+39	–519/+44
Subsurface (octahedral)	–519/+44	–565/–2	–596/–33	–616/–53 ^b
<i>Stepped surface</i>				
Coverage	25%	50%		
Step site (B5)	–651/–88	–590/–27		
Subsurface (near edge octahedral)		–550/+13		
Near edge (hcp hollow)	–543/+20	–588/–25 ^c		
Near edge (fcc hollow)		–540/+23		

^a Gibbs free energy for $1/2 \text{ B}_2\text{H}_6 (\text{g}) \leftrightarrow \text{B}^* + 3/2 \text{ H}_2 (\text{g})$ at FTS conditions.

^b Induces a surface reconstruction by boron–boron pair interactions.

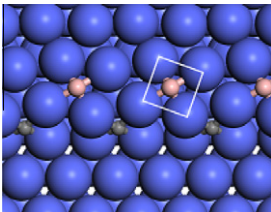
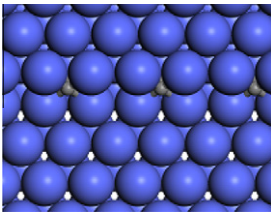
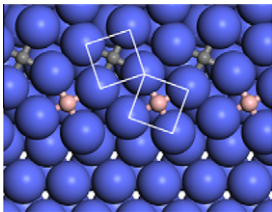
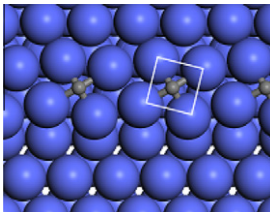
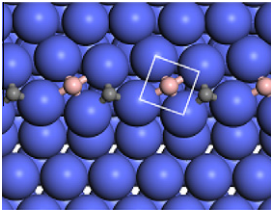
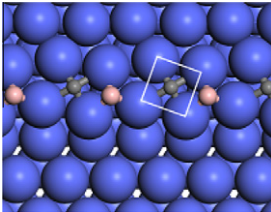
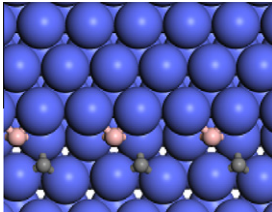
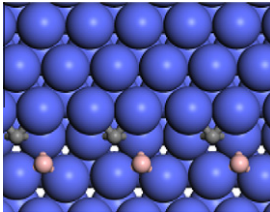
^c Induces a p4g clock reconstruction.

Table 2
Boron binding energies and Gibbs free reaction energies under FTS conditions, ΔG_r (500 K, 20 bar), (kJ/mol) for adsorption on a stepped $p(2 \times 8)$ Co unit cell.

Two boron atoms/unit cell Step and clock  –603/–40 ^a	Clock  –611/–48 ^a	Three boron atoms/unit cell Step and clock  –613/–50 ^a	Clock  –618/–55 ^a
Four boron atoms/unit cell Step and clock  –618/–55 ^a	Clock  –621/–58 ^a	Five boron atoms/unit cell Step and clock  –620/–57 ^a	Clock  –622/–59 ^a
Five rows of boron atoms/unit cell Subsurface octahedral  –617/–54 ^a		Five rows of boron atoms/unit cell Step and subsurface octahedral  –607/–44 ^a	

^a Binding energy/Gibbs free energy for $1/2\text{B}_2\text{H}_6(\text{g}) \leftrightarrow \text{B}^* + 3/2\text{H}_2(\text{g})$ at FTS conditions.

Table 3
Effect of boron on the carbon binding energies and stabilities under FTS conditions, ΔG_r (500 K, 20 bar), (kJ/mol) at nearby step and p4g clock sites on a stepped $p(2 \times 8)$ Co surface.

Carbon at a step site With boron  –555/+99 ^a	Without boron  –715/–61 ^a	Carbon at a clock site With boron  –589/+65 ^a	Without boron  –697/–43 ^a
Carbon and boron at p4g clock and step edge  –1188/–31 ^b	 –1142/+15 ^b	Carbon and boron at step and hcp hollow  –1199/–42 ^b	 –1189/–32 ^b

^a Carbon binding energy/Gibbs free energy for $\text{CO}(\text{g}) + \text{H}_2(\text{g}) \leftrightarrow \text{C}^* + \text{H}_2\text{O}(\text{g})$.

^b Combined boron and carbon binding energy/Gibbs free energy for $\text{CO}(\text{g}) + 1/2\text{B}_2\text{H}_6(\text{g}) \leftrightarrow \text{C}^* + \text{B}^* + 1/2\text{H}_2(\text{g}) + \text{H}_2\text{O}(\text{g})$.

The calculations reveal a strong similarity between carbon and boron adsorption on Co catalysts. Carbon at the step sites is more

stable than a single row of carbon at the near-edge p4g clock sites, but the stability of p4g carbon increases by 55 kJ/mol for a more

extended p4g reconstruction. The same trend is found for boron, and an extended p4g clock reconstruction is 40 kJ/mol more stable than boron at the step sites. The thermodynamic stability of the p4g clock boride under FTS conditions and the similarity between boron and carbon adsorption indicate that blocking the near-edge sites with boron before exposure to carbon might affect the adsorption and formation of resilient carbon deposits.

The effect of boron at the p4g sites on the stability of carbon at nearby sites is evaluated next (Table 3). The presence of boron at the near-edge p4g sites is calculated to reduce the binding energy of carbon at the nearby step sites by 160 kJ/mol. This makes the adsorption of carbon species at the step sites unfavorable under FTS conditions. Note that a row of carbon at the near-edge p4g clock sites increases the stability of carbon at the step sites by 56 kJ/mol [9]. To illustrate the effect of boron at the near-edge p4g clock sites, a carbon atom was initially adsorbed on the lower terrace of a stepped $p(2 \times 8)$ surface and then moved toward the step edge. The binding energy of -664 kJ/mol at the lower terrace is quite similar to the value of -658 kJ/mol for a 3-layered slab (Table 2, Tan et al., [9]). Next, the carbon atom was moved from the lower terrace toward the clean B5 step site, and the binding energy increases to -715 kJ/mol (Table 3, Tan et al., [9]). Next, these calculations were repeated on a stepped surface modified by a row of near-edge p4g carbon atoms. For this surface, the carbon binding energy on the lower terrace is also -664 kJ/mol. However, the binding energy increases by 107 kJ/mol to -771 kJ/mol when the carbon atom moves from the lower terrace to step site modified by p4g carbon atoms. Finally, this calculation was repeated for a stepped surface modified by p4g boron atoms. The carbon binding energy on the lower terrace remains at -664 kJ/mol. However, in the presence of boron at the p4g sites, the carbon binding energy decreases by 109 kJ/mol to -555 kJ/mol when the carbon atom is moved from the lower terrace to the step site (Table 3), indicating that the presence of boron at the near-edge p4g clock sites destabilizes carbon deposition at the B5 step sites. The effect of boron and carbon at the near-edge p4g sites on the carbon binding energy can be understood using the d-band model [50]. The higher carbon binding energy at the step sites relative to the terrace sites follows from the higher d-band center at the step edges. Reconstruction of the step edges to form a p4g clock carbide structure further increases the d-band center by 0.06 eV, leading to a 56 kJ/mol increase in the carbon binding energy. However, boron at the p4g clock sites shifts the d-band center away from the Fermi level by about 0.5 eV, thereby decreasing the carbon binding energy by 160 kJ/mol. The different effect of carbon and boron at the p4g sites can be understood from the charge density on the Co atoms at the step edges. Carbon is more electronegative than boron, and carbon withdraws 0.6 electrons more from the step edge Co atoms than boron. The increased charge density on the step Co atoms next to boron leads to a lower d-band center and hence a lower carbon binding energy. The calculations further indicate that the presence of boron atoms at the p4g clock sites reduces the stability of carbon at nearby clock sites by 108 kJ/mol, and carbon adsorption at nearby p4g clock sites also becomes thermodynamically unfavorable. Again, this trend follows from a downward shift in the center of Co d-band in the presence of boron. In addition to blocking sites for the adsorption of resilient carbon species, boron is hence predicted to destabilize carbon adsorption at nearby sites.

Finally, to evaluate whether boron is stable at the p4g clock and step sites in the presence of carbon, we compared the stability of a configuration with boron at the p4g site and carbon at a nearby terrace site with the inverse configuration (Table 3). First, it should be noted that removing boron from step, subsurface, or p4g clock sites to gas phase B_2H_6 is unfavorable by about 60 kJ/mol (Tables 1 and 2). Though surface CH^* and CH_2^* species can gain about 80 kJ/mol in stability by moving to the p4g clock sites [9], this process is likely

associated with a kinetic barrier because of the low stability of carbon near p4g boron species and the low stability of surface boron species. Indeed, the configuration with boron at the p4g site and carbon at a nearby fcc terrace site is 53 kJ/mol less stable than the configuration in which they are well-separated. The former configuration is also 46 kJ/mol more stable than the configuration with carbon at the p4g site and boron at the nearby fcc terrace site (Table 3). A similar preference is found when the stability of boron at the step edge and carbon at the nearby hollow site is compared with the inverse configuration. The calculations hence suggest that a p4g surface cobalt boride is stable under FTS conditions and that displacement of boron atoms by surface carbon atoms is thermodynamically unfavorable.

To evaluate the predicted effect of a boron promoter on the deposition of resilient carbon species, a series of boron-promoted Co catalysts was characterized using XPS, TPR, hydrogen chemisorption and CO DRIFTS, and finally tested during FTS. After reaction, the catalysts were characterized using XPS and TPH to evaluate the amount and the nature of the resilient carbon species formed on the Co catalyst, and using ICP-OES to confirm that there was no loss of the boron promoter.

3.2. Catalyst characterization

First, the effect of boron on the reducibility of the 20 wt.% Co/ γ - Al_2O_3 catalysts is evaluated. The TPR profiles in Fig. 1 are typical for Co catalysts promoted with small amounts of Pt to enhance their reducibility [7,9,37]. A low- and a high-temperature reduction peak were observed for all catalysts. However, the position and the magnitude of the peaks depend on the boron concentration. The TPR profile of Co/ γ - Al_2O_3 catalysts has been well characterized, and the reduction peaks at 260 °C and at 440 °C correspond to a two-step reduction process [37]. The first peak is often attributed to the reduction of Co_3O_4 to CoO, while the second peak corresponds to the reduction of CoO to metallic Co. The TPR profiles indicate that a reduction temperature above 500 °C might be required to fully reduce the Co catalysts, in particular for higher boron concentrations. In supported Co catalysts, the formation of cobalt-support compounds can affect the reducibility of the Co catalyst [51], leading to high-temperature reduction peaks (>800 °C) in the TPR spectra. However, our TPR profiles of boron-promoted and unpromoted Co/ γ - Al_2O_3 catalysts did not show such high-temperature peaks. The TPR profile of the Co/ γ - Al_2O_3 catalyst promoted with 0.5 wt.% boron closely resembles the profile of the unpromoted catalyst, except for a slight increase in reduction temperatures. Promotion with 2.0 wt.% boron has a more significant effect on the reduction profile and seems to decrease the reducibility of the Co catalyst. H_2 chemisorption measurements taken after reduction in flowing H_2 for 2 h at 500 °C confirm that promotion

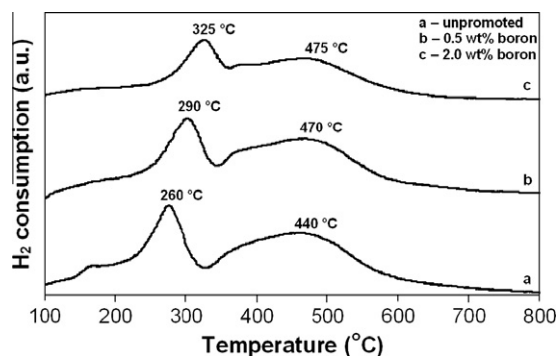


Fig. 1. Effect of boron promotion on the temperature-programmed reduction profile of 20 wt.% Co/ γ - Al_2O_3 catalysts.

with 2.0 wt.% boron reduces the hydrogen uptake by 25%, while promotion with 0.5 wt.% boron changes the hydrogen uptake by less than 10% (Table 4).

This observation is further supported by the CO DRIFT spectra shown in Fig. 2. The CO stretching peak near 2045 cm^{-1} is characteristic for CO adsorption at metallic Co sites [52]. Promotion with boron leads to a modest 5 cm^{-1} shift in the peak position, indicating that boron has a limited effect on the nature of the CO adsorption sites. However, a higher boron concentration significantly reduces the intensity of the DRIFT spectra (Fig. 2 and Table 4). This reduction is possibly caused by the lower number of available metallic Co sites for catalysts with 2.0 wt.% boron, as suggested by the lower reducibility observed in TPR and the reduced hydrogen uptake.

The effect of boron on the dispersion and particle size was also estimated from H_2 chemisorption data and from XRD (Table 4). An average Co particle size of 14 nm was determined for all catalysts by XRD, and this value did not change significantly with boron promotion. This is not unexpected since boron was introduced in a separate, second impregnation step, after calcination of the catalysts. The average particle size determined by H_2 chemisorption for the unpromoted Co catalyst, 11 nm, is slightly smaller than the value obtained by XRD, suggesting a nearly complete reduction of the Co particles. The particle size determined by H_2 chemisorption increases slightly for 0.5 wt.% boron, and increases to 14 nm for 2.0 wt.% boron, indicating that the H_2 uptake is reduced for higher boron concentrations. This is consistent with the TPR profiles that showed a lower reducibility of the Co catalysts with 2.0 wt.% boron.

Finally, the nature of the boron promoter after reduction of the catalysts for 2 h in flowing H_2 at 500 °C was investigated using XPS. XPS spectra for three samples are shown in Fig. 3; a 20 wt.% Co/ $\gamma\text{-Al}_2\text{O}_3$ catalyst promoted with 0.5 wt.% boron, a Co/ $\gamma\text{-Al}_2\text{O}_3$ catalyst promoted with 2.0 wt.% boron to enhance the B 1s XPS signal, and a $\gamma\text{-Al}_2\text{O}_3$ support loaded with 2.0 wt.% boron as a reference sample. All three samples were prepared and reduced following the procedure described in Section 2. The reference 2.0 wt.% B/ $\gamma\text{-Al}_2\text{O}_3$ sample shows a single B 1s peak at 191.0 eV, characteristic for a boron oxide [53]. A similar peak is observed for the promoted Co/ $\gamma\text{-Al}_2\text{O}_3$ catalysts. However, a shoulder at a lower binding energy is also observed for the promoted catalysts. Deconvolution of the XPS signal for the catalyst with 2.0 wt.% boron leads to a second peak with a B 1s binding energy of about 188.1 eV. The binding energy for this new peak is characteristic for a reduced cobalt boride phase and agrees with the binding energy reported for Co_2B , 188.1 eV [49]. Note however that bulk cobalt boride, Co_2B , is calculated to be about 30 kJ/mol less stable than the surface p4g cobalt boride. To help identify the nature of this reduced boron species, B 1s core level binding energies were calculated for the different forms of adsorbed boron discussed in the previous section. A boron 1s core level binding energy of 187.8 eV was calculated for the extended p4g cobalt boride, and the surface cobalt boride is hence a likely

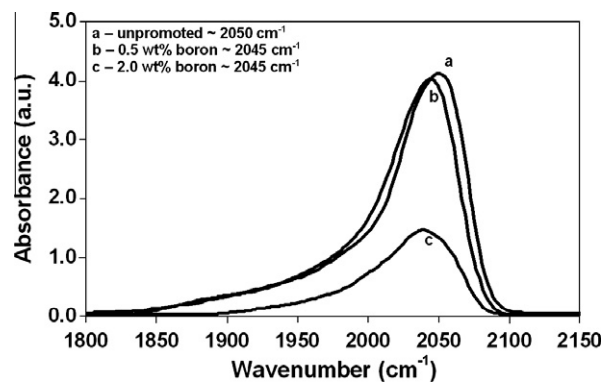


Fig. 2. Effect of boron promotion on the CO DRIFT spectra after exposure of 20 wt.% Co/ $\gamma\text{-Al}_2\text{O}_3$ catalysts to a 2% CO/Ar mixture at atmospheric pressure and 25 °C.

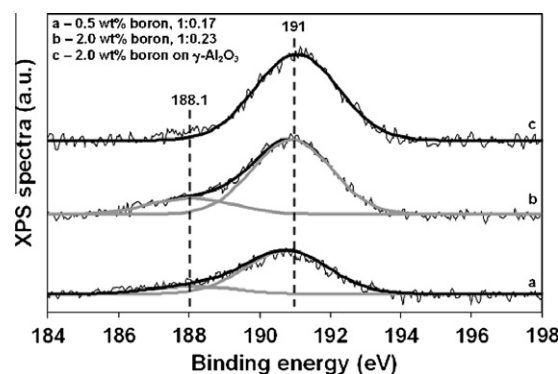


Fig. 3. Boron 1s XPS spectra for boron-promoted 20 wt.% Co/ $\gamma\text{-Al}_2\text{O}_3$ catalysts and for a reference $\gamma\text{-Al}_2\text{O}_3$ support impregnated with 2.0 wt.% boron, after reduction in 50 Nm³/min H_2 at 500 °C. The experimental signal (—) has been deconvoluted using Gaussian profiles (— and —) centered at the position of boron oxide (191.0 eV [53]) and Co boride (Co_2B , 188.1 eV [49]). The relative integrated intensities of the peaks are indicated.

candidate for the observed cobalt boride species. Boron at the step sites has a calculated B 1s core level binding energy of 186.5 eV, while the value for a monolayer of subsurface boron is 187.0 eV. The latter values are somewhat lower than the B 1s binding energy in the XPS spectra. The relative integrated intensities suggest that about 15% of the surface boron is reduced for the catalyst with 0.5 wt.% boron and about 19% for the catalyst with 2.0 wt.% boron. The observed partial reduction of the boron promoter is consistent with values reported by Xu et al. for supported Ni/ $\gamma\text{-Al}_2\text{O}_3$ catalysts promoted with 1.0 wt.% boron [27]. Since boron belongs to the group of Al, boron oxide can be expected to interact strongly with the $\gamma\text{-Al}_2\text{O}_3$ support, and therefore only boron atoms interacting with Co particles can be reduced. Note that 15% of 0.5 wt.% boron

Table 4
Particle size, dispersion, hydrogen uptake, normalized CO DRIFTS intensity, and hydrocarbon selectivity after 24 h for 20 wt.% Co/ $\gamma\text{-Al}_2\text{O}_3$ catalysts, promoted with different amounts of boron.

Promoter concentration	H_2 chemisorption			XRD		CO drifts	FT hydrocarbon selectivities (%)		
	H_2 uptake ($\mu\text{mol/g}_{\text{cat}}$)	Dispersion ^a (%)	$d(\text{Co})$ (nm)	$d(\text{Co}_3\text{O}_4)^b$ (nm)	$d(\text{Co})^c$ (nm)	Relative intensity	C ₁	C ₂₋₄	C ₅₊
Unpromoted	161	9.5	10.5	18.2	13.6	1.00	24	16	60
0.5 wt.% B	148	8.7	11.4	18.9	14.2	0.97	23	17	61
2.0 wt.% B	121	7.2	13.9	18.7	14.1	0.38	37	31	32

^a Dispersion determined from the H_2 uptake data using Eq. (6).

^b $d(\text{Co}_3\text{O}_4)$ determined using Scherrer's equation.

^c $d(\text{Co})$ is determined using Eq. (7).

corresponds to an equivalent Co coverage of 0.2 ML for a 20 wt.% Co/ γ -Al₂O₃ catalyst with a dispersion of 9.5%, and should hence be sufficient to occupy the near-edge p4g sites of the Co catalysts.

The characterization studies suggest that promotion with 0.5 wt.% boron has only a modest effect on the reducibility, the hydrogen uptake, and the CO chemisorption for a 20 wt.% Co/ γ -Al₂O₃ catalyst. Reduction at 500 °C converts about 15% of the boron oxide to a surface Co boride, leading to an equivalent boron coverage of 0.2 ML on the Co particles. Promotion with 2.0 wt.% boron affects the catalyst properties more drastically and is expected to change the FTS activity and selectivity.

3.3. Effect of boron promotion on the catalyst activity, selectivity, and stability

The FTS activity, selectivity, and stability of the Co catalysts were evaluated for 200 h at 240 °C, 20 bar and a H₂/CO ratio of 2. Fig. 4 shows the effect of boron promotion on the CO conversion as function of time on stream. The hydrocarbon selectivity after 24 h is given in Table 4. The temperature selected in our experiments is slightly higher than the temperature of 230 °C used to study catalyst deactivation in Sasol's demo-scale bubble column reactor [7,15], and somewhat higher than industrially used temperatures between 210 and 220 °C [2,8,13]. However, slightly higher temperatures are common in catalyst stability tests [40,42] and allow evaluation of the catalyst stability in a shorter period.

Promotion with 0.5 wt.% boron has a limited effect on the CO conversion and the C₅₊ selectivity during the first 30 h of time on stream (Table 4). During the first 24 h, the CO conversion increases from about 55% to 96% for the unpromoted catalyst and to 92% for the promoted catalyst. The initial increase in the activity might be

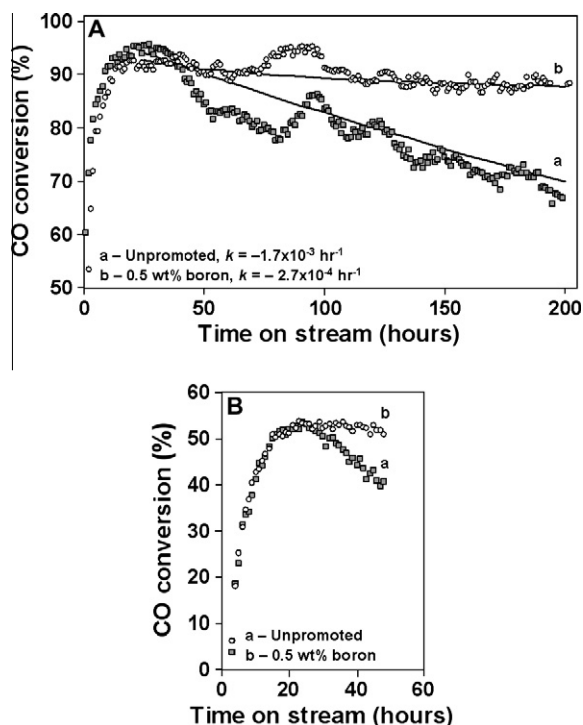


Fig. 4. Effect of boron promotion on the CO conversion as a function of time on stream for a 20 wt.% Co/ γ -Al₂O₃ FTS catalyst. (A) Long-term stability test. Reaction conditions: 240 °C, 20 bar, H₂/CO ratio of 2.0, $W_{\text{cat}}/F_{\text{total}} = 7.5 \text{ g}_{\text{cat}} \text{ h/mol}$, and duration of 200 h. The decrease in conversion is described by a first-order deactivation model (—), and the first-order deactivation rate coefficients, k , are indicated. (B) To evaluate the effect of boron promotion on the FTS activity and selectivity at lower CO conversion, the catalysts were evaluated using a lower space time, $W_{\text{cat}}/F_{\text{total}} = 3.8 \text{ g}_{\text{cat}} \text{ h/mol}$, for 48 h.

due to a further reduction and/or a surface reconstruction of the Co catalyst under reducing syngas conditions [6,54], as well as the reactor hydrodynamics. Using the dispersions reported in Table 1, a reactor average CO turnover frequency (TOF) of $3.7 \times 10^{-2} \text{ s}^{-1}$ was calculated for both catalysts. This value is comparable with the TOFs reported in the review by Ribeiro et al. [55]. Using the power law kinetic model proposed by Ribeiro et al., the TOF reported for a 15 wt.% Co/ γ -Al₂O₃ catalyst at 215 °C and 8.2 bar can be extrapolated to a value of $2.5 \times 10^{-2} \text{ s}^{-1}$ for our reaction conditions [55]. A significantly lower maximum CO conversion of 31% was obtained for Co catalysts promoted with 2.0 wt.% boron. This lower activity is consistent with the reduction in the number of active sites as indicated by the TPR, CO DRIFTS, and H₂ chemisorption data.

For the unpromoted catalyst, the CO conversion decreased rapidly from a maximum value of 96% to 81% after 50 h on stream and more gradually to 67% after 200 h. The overall deactivation behavior can be described by a first-order deactivation model with a rate coefficient of $1.7 \times 10^{-3} \text{ h}^{-1}$ [9]. At 230 °C, Saib et al. [7] observed a 20% decrease in activity during the first 200 h of their 55-day experiment in a 100 barrels/day demo-scale bubble column reactor, slightly lower than the deactivation rate measured here at 240 °C. In contrast, the catalyst promoted with 0.5 wt.% boron deactivates much more slowly. The CO conversion of 88% after 200 h is only marginally lower than the maximum CO conversion of 92%. The deactivation of the promoted catalyst can be described by a first-order deactivation rate coefficient of $2.7 \times 10^{-4} \text{ h}^{-1}$, a more than 6-fold decrease compared to the unpromoted catalyst. Promotion with 0.5 wt.% boron however did not affect the product distribution (Table 4). Methane selectivity was slightly high at 23%, but consistent with a reaction temperature of 240 °C [9]. Promotion with 2.0 wt.% boron not only reduced the CO conversion, but also reduced the C₅₊ selectivity from 60% to 32%. To confirm that promotion with 0.5 wt.% boron does not affect the FTS activity or selectivity, additional experiments at a lower space time, $W_{\text{cat}}/F_{\text{total}} = 3.8 \text{ g}_{\text{cat}} \text{ h/mol}$, were performed (Fig. 4B). After 25 h, the unpromoted Co catalyst reached a maximum CO conversion of 54% with a CH₄ selectivity of 27% and a chain growth probability of 0.7. After 25 h, the Co catalyst promoted with 0.5 wt.% boron reached a maximum CO conversion of 53% with a CH₄ selectivity of 26% and a chain growth probability of 0.7. During the first 30 h, the promoted and unpromoted catalysts are nearly indistinguishable. The decrease in the maximum CO conversion from 96% to 54% when the space time is halved is moreover consistent with an overall near-first-order kinetic model [55,56]. After 30 h, the unpromoted catalyst begins to deactivate and the CO conversion decreases to 41% after 48 h. In contrast, the promoted catalyst does not show any significant deactivation during the experiment. Note that the deactivation of the unpromoted Co catalysts during the 48 h experiment in Fig. 4B corresponds to the fast deactivation phase and might not be representative for the long-term deactivation behavior at those conditions.

To evaluate the effect of boron promotion on the nature and the amount of deposited carbon, both catalysts were characterized using TPH and C 1s XPS after 200 h on stream. TPH profiles and C 1s XPS data are shown in Fig. 5. Using TPH, different forms of resilient carbon can be distinguished, based on their reactivity toward hydrogen [9,15,57–60]. The low temperature peak for the unpromoted catalyst has been attributed to hydrocarbon waxes remaining after wax extraction, while surface and bulk carbides are predicted to undergo hydrogenation at higher temperatures [9,15,57–59]. The resilient carbon deposits that hydrogenate above 400 °C have been attributed to amorphous and poly-aromatic carbon species [9,60]. Such carbon deposits were also identified using TEM on the unpromoted catalyst after 200 h of reaction [9,15]. Similar lamellar carbon deposits could not be found on the

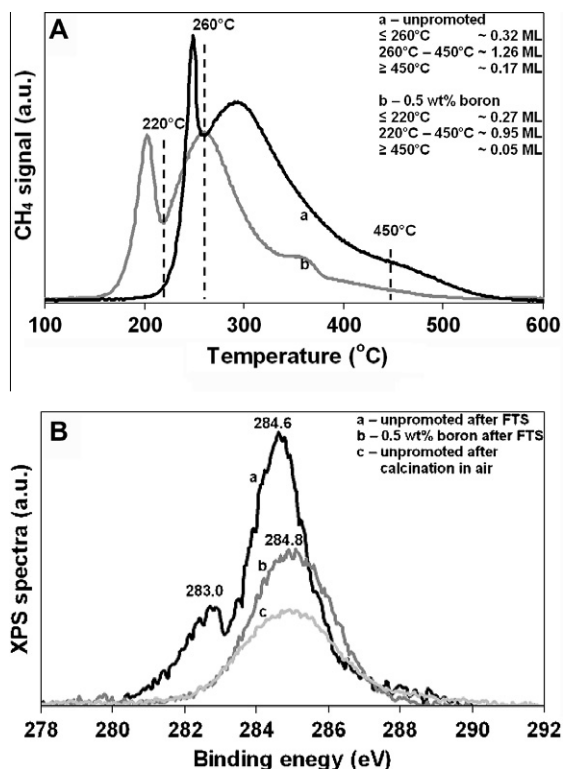


Fig. 5. Catalyst characterization after 200 h of FTS. (A) TPH profiles for an unpromoted (—) and boron-promoted (—) 20 wt.% Co/ γ -Al₂O₃ catalyst. The corresponding coverages for weakly adsorbed, intermediate, and resilient carbon species are indicated. (B) C 1s XPS spectra for an unpromoted (—) and a boron-promoted (—) catalyst, after wax extraction. The spectrum for a calcined, unpromoted catalyst (—) is provided for reference. The peak around 284.6 eV can be attributed to a combination of amorphous and poly-aromatic carbon species [9,64], while the peak around 283.0 eV corresponds to a Co carbide phase [9,62].

boron-promoted catalysts. Though the temperature at which different carbon species undergo hydrogenation is kinetically determined, the calculated relative stability of surface CH₂^{*} species, a p4g surface carbide phase, and extended graphene islands can be converted to temperature shifts of approximately 100 °C and 250 °C. This corresponds reasonably well with the temperature differences observed in TPH [9]. The amount of carbon that hydrogenates below 260 °C corresponds to an equivalent carbon coverage of about 0.32 ML, while an equivalent coverage of 1.26 ML is calculated for carbon species that hydrogenate between 260 and 450 °C. About 0.17 ML of highly resilient carbon species are detected on the unpromoted Co catalyst after 200 h on stream. Promotion with 0.5 wt.% boron reduces the total amount of carbon by about 30%. Boron promotion also shifts the peak temperatures to lower temperatures and reduces the amount of highly resilient carbon species that hydrogenate above 450 °C from 0.17 ML to 0.05 ML. Unfortunately, since surface carbonaceous species are both reaction intermediates and a possible cause of deactivation during FTS, correlating the total amount of deposited carbon determined by TPH with the observed catalyst deactivation rate is less straightforward than for methane steam reforming over Ni catalysts [27]. For Ni catalysts, promotion with 1.0 wt.% boron was found to reduce the deactivation rate by a factor of 3 and the amount of deposited carbon by a factor of 5 [27]. However, the amount of highly resilient carbon species that hydrogenates above 450 °C can be related to the observed catalyst deactivation. Indeed, in their study of the deactivation of supported Co catalysts in a slurry bubble column reactor, Moodley et al. were able to correlate the amount of resilient carbon that hydrogenates above 400 °C with the loss in catalyst activity [15]. In our study, the 3-fold reduction

in the amount of carbon that hydrogenates above 450 °C correlates reasonably well with the observed 6-fold reduction in the deactivation rate for the promoted Co catalysts. The downward shift in the initial hydrogenation temperature for the promoted catalyst may be due to a higher remaining hydrogenation activity of the promoted catalyst. A similar gradual increase in the initial hydrogenation temperature with time on stream was also reported by Moodley et al. [15]. To evaluate the possibility of catalyst sintering, the Co particle size and dispersion were determined after reaction using H₂ chemisorption for the unpromoted catalyst [9]. Deposited carbon species were removed by hydrogenation at 500 °C for 2 h under 50 Nml/min H₂ before performing the H₂ adsorption isotherms. The hydrogen uptake decreased slightly from 161 to 134 μ mol/g_{cat} [9]. Though this could correspond to a 10% increase in the average particle size, the decreased hydrogen uptake might well be due to an incomplete removal of the carbon deposits after hydrogenation at 500 °C, as shown by the TPH profiles for the unpromoted catalyst (Fig. 5A).

Boron promotion also affects the C 1s XPS spectra of the catalysts after reaction. The spectrum of the unpromoted catalyst in Fig. 5B shows C 1s peaks at 283.0 and 284.6 eV. The lower intensity peak at 283.0 eV can be attributed to cobalt carbide [9,61,62] and is fairly close to values reported for a p4g clock reconstructed carbide on Ni(1 0 0) [63]. The binding energy also corresponds well with the core level binding energy of 283.4 eV calculated using DFT-PBE for a p4g clock Co carbide [9]. The peak at 284.6 eV can be assigned to amorphous and poly-aromatic carbon [64,65], but may also include long-chain hydrocarbon products remaining on the catalyst surface after wax extraction [66]. The reported XPS binding energy for surface CH₂^{*} species on Co(1 1 1), 284.9 eV, [67] is indeed only slightly higher than the value for graphitic carbon, 284.6 eV. Thus, these species cannot be easily distinguished by XPS. Promotion with 0.5 wt.% boron reduces the overall XPS intensity, and the carbide peak at 283.0 eV can no longer be detected. The peak at 284.6 eV shifts to a higher binding energy of 284.8 eV and has a slightly different shape. This peak might correspond to poly-aromatic carbon species, though the higher binding energy could also correspond to hydrocarbon products remaining on the catalyst surface after wax extraction [66]. Note that even for a pristine and calcined Co catalyst, a C 1s peak at 284.8 eV is found. This peak has been attributed to typical carbon contamination inside the XPS chamber [68].

4. Conclusions

Supported Co catalysts show a gradual loss in activity during FTS. This deactivation can, in part, be attributed to the deposition of resilient carbon species. Detailed DFT-PBE calculations indicate that the relative stability of boron on Co terraces and near Co step sites mimics the relative stability of carbon species on the same surfaces. Similar to carbon, boron is calculated to bind strongly at the step sites and to induce a p4g clock reconstruction growing from the step edges. Both forms of boron are thermodynamically more stable than boron oxide (B₂O₃) and diborane (B₂H₆) under FTS conditions. The presence of boron atoms at the step and p4g clock sites also reduces the stability of carbon at nearby sites by shifting the d-band center away from the Fermi level. In addition, the displacement of boron atoms at clock and step sites by surface carbon atoms is thermodynamically unfavorable. Hence, a surface cobalt boride is predicted to be thermodynamically stable during FTS, and small amounts of boron are proposed to selectively prevent the adsorption of resilient carbon species near the step edges, which might prevent catalyst deactivation.

To evaluate the predicted effect, 20 wt.% Co/ γ -Al₂O₃ catalysts were promoted with 0.5 and 2.0 wt.% boron, carefully

characterized, and tested during FTS in a fixed bed micro-reactor at 240 °C and 20 bar for 200 h. Characterization indicates that 0.5 wt.% boron has a limited effect on the reducibility of the Co catalyst and on the nature and the number of the H₂ and CO adsorption sites. Higher boron concentrations significantly decrease catalyst reducibility. Promotion with 0.5 wt.% boron does not affect the maximum activity and the C₅₊ selectivity of the Co catalyst. However, the unpromoted Co catalyst gradually deactivates and loses about 30% of its maximum activity after 200 h. In contrast, the boron-promoted catalyst retains more than 95% of its maximum activity after 200 h on stream. TPH and XPS characterization shows that boron promotion reduces the amount of resilient carbon deposits more than 3-fold and likely prevents the formation of surface cobalt carbide.

Acknowledgments

Financial support from the Agency for Science, Technology and Research (A-Star Project 062-101-0035), and from the National University of Singapore are gratefully acknowledged. The authors would like to thank Dr. Xu Jing and Grace Li Xian Mok for their contributions during the initial phase of this project.

References

- [1] M.E. Dry, *Appl. Catal. A* 138 (1996) 319.
- [2] E. Iglesia, *Appl. Catal. A* 161 (1997) 59.
- [3] R.B. Anderson, *The Fischer–Tropsch Synthesis*, Academic Press, New York, 1984.
- [4] B.H. Davis, *Ind. Eng. Chem. Res.* 46 (2007) 8938.
- [5] A.M. Saib, D.J. Moodley, I.M. Ciobica, M.M. Hauman, B.H. Sigwebela, C.J. Weststrate, J.W. Niemantsverdriet, J. Van de Loosdrecht, *Catal. Today* 154 (2010) 271.
- [6] N.E. Tsakoumis, M. Rønning, Ø. Borg, E. Rytter, A. Holmen, *Catal. Today* 154 (2010) 162.
- [7] A.M. Saib, A. Borgna, J. van de Loosdrecht, P.J. van Berge, J.W. Niemantsverdriet, *Appl. Catal. A* 312 (2006) 12.
- [8] P.J. van Berge, R.C. Everson, *Stud. Surf. Sci. Catal.* 107 (1997) 207.
- [9] K.F. Tan, J. Xu, J. Chang, A. Borgna, M. Saeys, *J. Catal.* 274 (2010) 121.
- [10] S.L. Soled, E. Iglesia, R.A. Fiato, G.B. Ansell, United States Patent 5397,806, 1995 (to Exxon).
- [11] M.J. van der Burgt, J. Ansoorge, Great Britain Patent 2222,531, 1988 (to Shell).
- [12] H.A. Wright, United States Patent 6486,220 B1, 2002 (to Conoco).
- [13] E. Iglesia, S.L. Soled, R.A. Fiato, G.H. Via, *J. Catal.* 143 (1993) 345.
- [14] J. Lahtinen, G.A. Somorjai, *J. Mol. Catal. A* 130 (1998) 255.
- [15] D.J. Moodley, J. van de Loosdrecht, A.M. Saib, M.J. Overett, A.K. Datye, J.W. Niemantsverdriet, *Appl. Catal. A* 354 (2009) 102.
- [16] J.J.H.M. Font Freide, T.D. Gamlin, R.J. Hensman, B. Nay, C. Sharp, *J. Nat. Gas Chem.* 13 (2004) 1.
- [17] A. Martínez, J. Rollán, M.A. Arribas, H.S. Cerqueira, A.F. Costa, E.F. S-Aguar, *J. Catal.* 249 (2007) 162.
- [18] O. Ducreux, J. Lynch, B. Rebours, M. Roy, P. Chaumette, *Stud. Surf. Sci. Catal.* 119 (1998) 125.
- [19] J.R. Rostrup-Nielsen, *J. Catal.* 85 (1984) 31.
- [20] H.S. Bengaard, J.K. Nørskov, J. Sehested, B.S. Clausen, L.P. Nielsen, A.M. Molenbroek, J.R. Rostrup-Nielsen, *J. Catal.* 209 (2002) 365.
- [21] F. Besenbacher, I. Chorkendorff, B.S. Clausen, B. Hammer, A.M. Molenbroek, J.K. Nørskov, I. Stensgaard, *Science* 279 (1998) 1913.
- [22] J.S. Choi, K.I. Moon, Y.G. Kim, J.S. Lee, C.H. Kim, D.L. Trimm, *Catal. Lett.* 52 (1998) 43.
- [23] J. Xu, M. Saeys, *J. Catal.* 242 (2006) 217.
- [24] L. Chen, Y. Lu, Q. Hong, J. Lin, F.M. Dautzenberg, *Appl. Catal. A* 292 (2005) 295.
- [25] F. Abild-Pedersen, O. Lytken, J. Engbæk, G. Nielsen, I. Chorkendorff, J.K. Nørskov, *Surf. Sci.* 590 (2005) 127.
- [26] J. Xu, M. Saeys, *J. Phys. Chem. C* 113 (2009) 4099.
- [27] J. Xu, L. Chen, K.F. Tan, A. Borgna, M. Saeys, *J. Catal.* 261 (2009) 158.
- [28] M. Saeys, K.F. Tan, J. Chang, A. Borgna, *Ind. Eng. Chem. Res.* 49 (2010) 11098.
- [29] J.P. Perdew, K. Burke, M. Ernzerhof, *Phys. Rev. Lett.* 77 (1996) 3865.
- [30] G. Kresse, J. Hafner, *Phys. Rev. B* 47 (1993) 558.
- [31] G. Kresse, J. Hafner, *Phys. Rev. B* 48 (1993) 13115.
- [32] P.E. Blöchl, *Phys. Rev. B* 50 (1994) 17953.
- [33] N.W. Ashcroft, N.D. Mermin, *Solid State Physics*, Holt, Rinehart and Winston, New York, 1976.
- [34] E. van Steen, M. Claeys, M.E. Dry, J. van de Loosdrecht, E.L. Viljoen, J.L. Visagie, *J. Phys. Chem. B* 109 (2005) 3575.
- [35] M.W. Chase, *J. Phys. J. Phys. Chem. Ref. Data* 9 (1998) 1 (Monograph).
- [36] L. Köhler, G. Kresse, *Phys. Rev. B* 70 (2004) 165405.
- [37] G. Jacobs, P.M. Patterson, Y. Zhang, T. Das, J. Li, B.H. Davis, *Appl. Catal. A* 233 (2002) 215.
- [38] D.E. Mears, *J. Catal.* 20 (1971) 127.
- [39] P. Zehner, E.U. Schlunder, *Chemie Ingr. Tech.* 42 (1970) 933.
- [40] Y. Zhang, Y. Liu, G. Yang, S. Sun, N. Tsubaki, *Appl. Catal. A* 321 (2007) 79.
- [41] N. Tsubaki, S. Sun, K. Fujimoto, *J. Catal.* 199 (2001) 236.
- [42] B.J. Cooper, D.L. Trimm, in: B. Delmon, G.F. Froment (Eds.), *Catalyst Deactivation*, vol. 6, Elsevier, Amsterdam, 1980.
- [43] G.V. Pankina, P.A. Chernavskii, A.S. Lermontov, V.V. Lunin, *Petrol. Chem.* 42 (2002) 217.
- [44] M. Boudart, G. Djega-Mariadassou, *Kinetics of Heterogenous Catalytic Reactions*, Princeton Univ. Press, Princeton, NJ, 1984, p. 26.
- [45] J.L. Lemaître, P.G. Menon, F. Delannay, F. Delannay (Eds.), *Characterization of Heterogeneous Catalysts*, vol. 15, Dekker, New York, 1984, p. 325.
- [46] E.J. Baum, *Chemical Property Estimation: Theory and Application*, Lewis Publishers, Boca Raton, 1998, p. 35.
- [47] J.H. Onuferko, D. P. Woodruff, B.W. Holland, *Surf. Sci.* 87 (1979) 357.
- [48] R.W.G. Wyckoff, *Crystal Structures*, vol. 1., Interscience Publishers, New York, 1960.
- [49] G. Mavel, J. Escard, P. Costa, J. Castaing, *Surf. Sci.* 35 (1973) 109.
- [50] B. Hammer, J.K. Nørskov, *Surf. Sci.* 343 (1995) 211.
- [51] B. Jongsoomjit, J. Panpranot, J.G. Goodwin, *J. Catal.* 204 (2001) 98.
- [52] F. Morales, E. de Smit, F.M.F. de Groot, T. Visser, B.M. Weckhuysen, *J. Catal.* 246 (2007) 91.
- [53] I. Jimenez, D.G.J. Sutherland, T. Van Burren, J.A. Carlisle, L.J. Terminello, *Phys. Rev. B* 57 (1998) 13167.
- [54] J. Wilson, C. de Groot, *J. Phys. Chem.* 99 (1995) 7860.
- [55] F.H. Ribeiro, A.E. Schach von Wittenau, C.H. Bartholomew, G.A. Somorjai, *Catal. Rev. Sci. Eng.* 39 (1997) 49.
- [56] G.F. Froment, K.B. Bischoff, *Chemical Reactor Analysis and Design*, second ed., John Wiley & Sons, New York, 1990, 84.
- [57] V. Gruver, R. Young, J. Engman, H.J. Robota, *Prep. Pap. Am. Chem. Soc., Div. Petrol. Chem.* 50 (2005) 164.
- [58] J. Xu, C.H. Bartholomew, *J. Phys. Chem. B* 109 (2005) 2392.
- [59] V. Gruver, X. Zhan, J. Engman, H.J. Robota, *Prep. Pap. Am. Chem. Soc. Div. Petrol. Chem.* 49 (2004) 192.
- [60] D.-K. Lee, J.-H. Lee, S.-K. Ihm, *Appl. Catal.* 36 (1988) 199.
- [61] G.A. Beitel, C.P.M. de Groot, H. Oosterbeek, J.H. Wilson, *J. Phys. Chem. B* 101 (1997) 4035.
- [62] G.A. Beitel, A. Laskov, H. Oosterbeek, E.W. Kuipers, *J. Phys. Chem.* 100 (1996) 12494.
- [63] N. Mårtensson, A. Nilsson, *J. Electron Spectrosc. Relat. Phenom.* 75 (1995) 209.
- [64] J.F. Moulder, *Handbook of X-ray Photoelectron Spectroscopy*, Perkin Elmer, Eden Prairie, 1982, p. 147.
- [65] F. Le Normand, J. Hommet, T. Szörénti, C. Fuchs, E. Fogarassy, *Phys. Rev. B* 64 (2001) 235416.
- [66] Z. Yan, Z. Wang, D.B. Bukur, D.W. Goodman, *J. Catal.* 268 (2009) 196.
- [67] F. Solymosi, I. Kovács, *Surf. Sci.* 296 (1993) 171.
- [68] M.Z. Atashbar, H.T. Sun, B. Gong, W. Wlodarski, R. Lamb, *Thin Solid Films* 326 (1998) 238.